Broadband cloaking using composite dielectrics

Ruey-Bing Hwang and Cheng-Yuan Chin

Citation: AIP Advances **1**, 012112 (2011); doi: 10.1063/1.3562891
View online: http://dx.doi.org/10.1063/1.3562891
View Table of Contents: http://scitation.aip.org/content/aip/journal/adva/1/1?ver=pdfcov
Published by the AIP Publishing

Broadband cloaking using composite dielectrics

Ruey-Bing Hwang[a] and Cheng-Yuan Chin
Department of electrical engineering, National Chiao Tung University, 1001 Ta-Hsueh Road, Hsinchu, Taiwan

(Received 15 December 2010; accepted 14 February 2011; published online 1 March 2011)

In this paper, we present a novel cloaking structure that is able to make a metallic block invisible in a metallic waveguide. Such a cloak is made up of a stack of commonly used dielectric slabs. We carry out the numerical simulation and observe the detour of the vector Poynting power through the cloak. Moreover, the experiment is conducted for measuring the scattering characteristics including the reflection and transmission coefficients. The great improvement in the transmission coefficient in a broad bandwidth after cloaking is demonstrated. Significantly, the theory of mode conversion is developed for explaining the cloaking phenomenon. [doi:10.1063/1.3562891]

I. INTRODUCTION

Cloaking or making arbitrary-shaped objects invisible from electromagnetic wave incidence has been the subject of continuing interest in microwave and physics communities. A rich variety of novel ideas and potential applications were proposed.[1–15] To mention a few, some researchers developed novel cloaking techniques based on several approaches, such as surface plasmon polariton,[1–3] anomalous localized resonances,[4,5] coordinate transformation such as conformal mapping[6,7] and transformation optics.[8–10]

The physical mechanism of cloaks in Ref. 1 relies on the effect that scattered wave from the cloak may cancel the one from the object to be cloaked, leaving the observer with very low residual scattering. For experimental studies, specific permittivity of plasmonic material is available for noble metal, such as silver and gold, in optical spectrum. However, an arbitrary permittivity of plasmonic material in microwave and millimeter wave is not available. Different from the coordinate-transformation-based technique, Milton *et al.* employed anomalous localized resonances to realize cloaking in the region external to the cloak.[5] However, the strong resonances are sensitive to losses and operating frequency. Moreover, this technique is under the quasi-static approximation and specific field polarization.

Recently, the coordinate-transformation-based technique has provided new tools to transform wave propagation using the invariance of Maxwell equations. The first experimental verification of metamaterial cloaking has been achieved at microwave frequencies in a two-dimensional environment.[10] Transformation-based cloaks deform the space around a given region for detouring the impinging rays around the region, and for prohibiting them from penetrating into the region. Distinct from the plasmonic cloaking, such a cloak creates the electromagnetic field isolation in the hidden region. Nevertheless, the cloak needs an ideal anisotropic and inhomogeneous medium, causing a narrow bandwidth response. Another approach for designing cloak presented is based on transmission-line networks that can be unloaded or periodically loaded by lumped elements.[11,12] The transmission-line network is in fishnet shape with the net composed of metal. The objects to be hidden are placed inside the grids. Different from transformation-based cloaks, the impinging

[a]Electronic mail: raybeam@mail.nctu.edu.tw

TABLE I. Parameters of dielectric slabs

Material	Relative Dielectric Constant	Length (mm)	Width (mm)
Acrylic	ϵ_1=2.1	l_1=27.0	w_1=10
FR4 epoxy	ϵ_2=4.4	l_2=51.6	w_2=10
RT6010	ϵ_3=10.5	l_3=79.5	w_3=10

wave propagates through the object instead of propagating around the object. A properly designed network may make large number of small particles invisible but a large bulky one.

In this paper, we present a microwave cloak made of composite dielectrics. Unlike the cloaking transformation, the cloaking structure consists only of conventionally used dielectric material. We put the cloaking structure inside a metallic waveguide to cloak a metallic block. By measuring the return- and insertion- loss (S_{11} and S_{21}), the broadband cloaking was observed. Parameter S_{11} is the reflection coefficient defined as the ratio of reflected- to incident- power at the input port of the waveguide when the output port is terminated with matched load. Parameter S_{21} is the transmission coefficient that can be found by applying an incident wave at the input port and measuring the outcoming wave at the output port. In addition to the numerical and experimental studies, the theory of mode conversion is employed to explain that cloaking structure can detour the propagation of electromagnetic wave.

II. STRUCTURE CONFIGURATION

Figure 1 shows the structure configuration of the dielectric cloak around a metallic block in a metallic waveguide, where (a) is the picture of the whole structure, (b) is the enlargement of the dielectric cloak, and (c) is the top view of the cloak. The dielectric cloak is composed of a stack of dielectric slabs with different relative dielectric constants and lengths. With the coordinate system attached, the cloak is symmetric with respect to the x- and y- axis, respectively. The thickness (the dimension along the z-axis) of the cloak is the same as the height of the waveguide. Notably, the dielectric media employed contain Acrylic, FR4 and RT6010, which are low loss dielectric substrate in the operational bandwidth.

The object to be cloaked is a metallic block with dimension $18.51\times18.51\times43$ mm^3, and is put at the center of the waveguide. Here, the waveguide is a modified aluminum WR-340 waveguide with the inside dimensions 86.36×43 mm^2. The operational bandwidth is from 2.2 GHz to 3.3 GHz for the TE_{10} mode. Additionally, the waveguide are equipped with the standard coaxial probes with height 24 mm. The distance from the waveguide (front and back) walls is 300 mm.

III. NUMERICAL AND EXPERIMENTAL RESULTS

We employ the commercial software (CST^{TM} - Microwave Studio) based on finite integration technique to optimize the parameters including the length and width of each dielectric slab for reducing the reflection and enhancing the transmission in a broad bandwidth. After the optimization process, we obtain the dielectric cloak with dimensions given in Table I.

Figure 2 shows the distribution of S_{21} against frequency for the three cases, which are bare waveguide, waveguide with the uncloaked object, and waveguide with the cloaked object, respectively. Apparently, the waveguide with uncloaked object exhibits a significant insertion loss. It is because that the presence of the metallic block opens the two new waveguides with the channel width 33.925 mm. Since their cutoff frequency of the fundamental mode is at 4.4215 GHz, the low transmission is attributed to the below-cutoff phenomenon of the two small waveguides. Interestingly, the cloaking structure can enhance the transmission at least 12 dB from 2.2 to 3.3 GHz. From the waveguide theory, we know that the multiple dielectric layers inserted in the small waveguide shall introduce a new fundamental mode with the cutoff frequency below the original one without

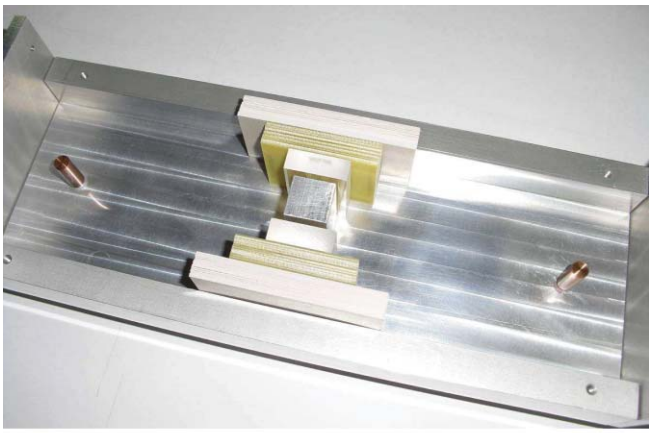

(a)

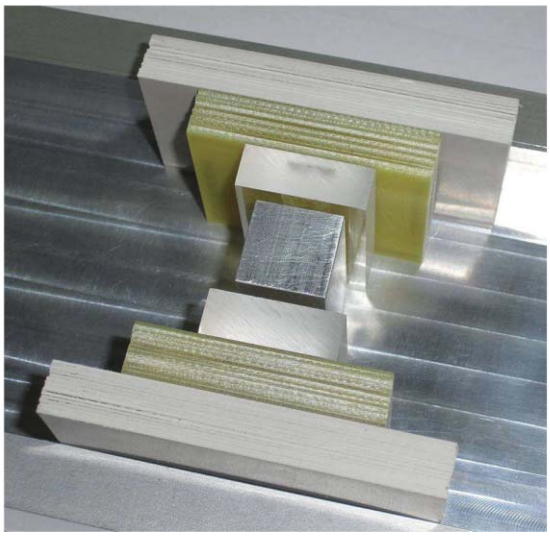

(b)

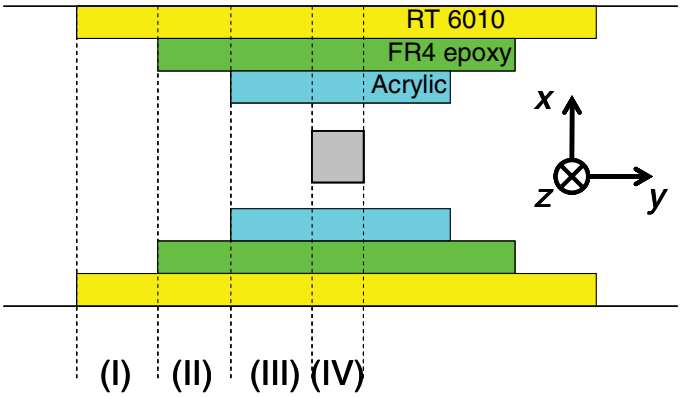

(c)

FIG. 1. Structure configuration: (a) picture of the whole structure, (b) enlargement of composite dielectrics and metallic block, (c) the four constituent regions for evaluating the dispersion characteristics.

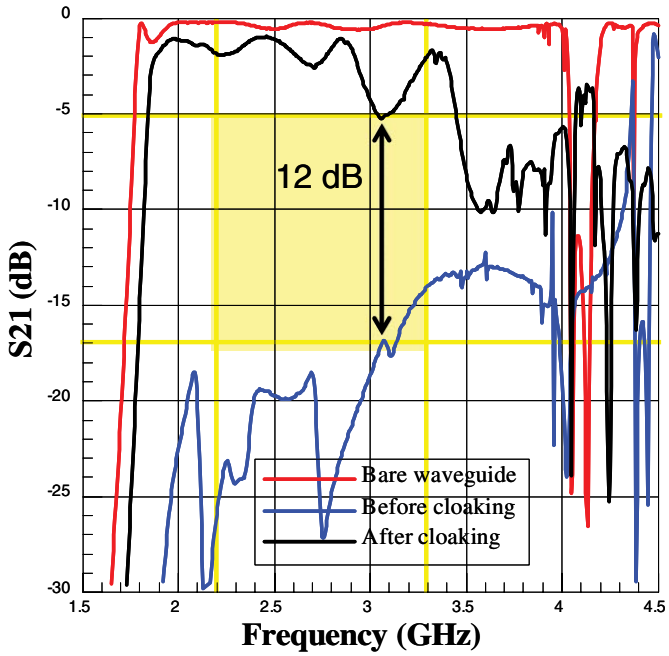

FIG. 2. Measured transmission coefficients of three cases: bare waveguide, waveguide with uncloaked object and waveguide with cloaked object. The dimension of metallic block is $18.51 \times 18.51 \times 43$ mm^3.

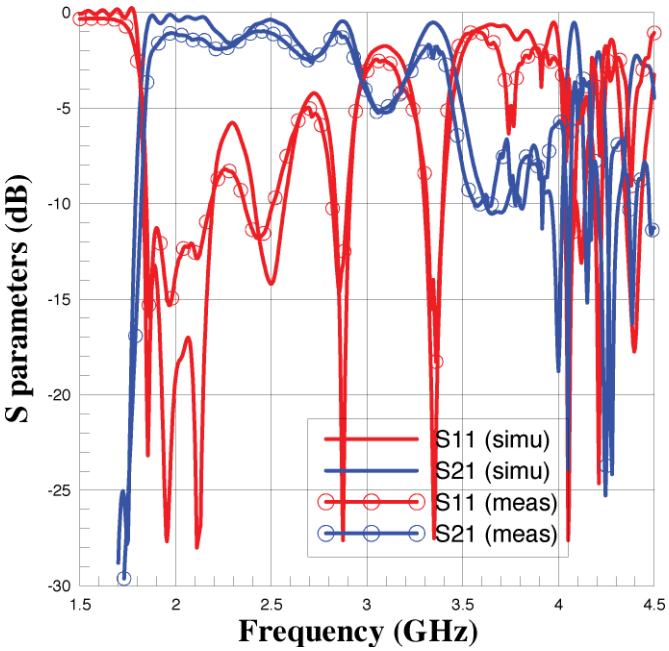

FIG. 3. Numerical and experimental results for waveguide with cloaked object.

filling dielectric medium. Such a mode can manipulate the wave propagation in the small waveguide, achieving the propagating path deformation.

Figure 3 depicts the calculated and measured scattering parameters including the S_{11} and S_{21}. The lines with symbol denote the measured results, while the others are calculated ones. Apparently, in general the good agreement between the simulated and measured results is observed.

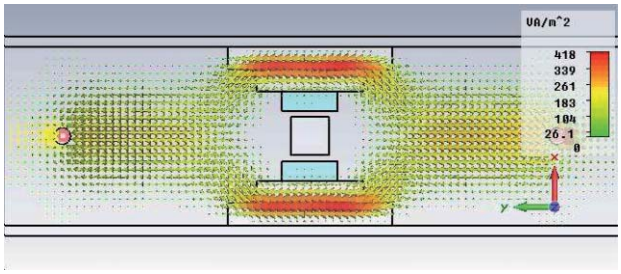

FIG. 4. Distribution of vectorized Poyting power in the entire structure.

IV. PHYSICAL CONSEQUENCE OF CLOAKING PHENOMENON

Additionally, we have calculated the distribution of the Poynting power density in the whole waveguide containing metal object and the dielectric cloak for investigating the physical picture of wave process involved in the cloaking structure. As shown in Fig. 4, the strength and direction of the arrow represent the Poynting power density at the observation point. The TE_{10} mode launched by the input probe has most of its power density concentrated in the central region. After hitting the cloaking structure, the locations of maximum power density will be gradually transferred to those near the waveguide sidewalls. Namely, the composite dielectrics cloak can detour the propagation path of the electromagnetic energy. Since the cloaking structure is symmetric with respect to the x-axis, the field can reverse the process and then converge to the receiving port.

From the Poynting power distribution, we certainly know that the cloaking is attributed to the detour of the electromagnetic energy propagation. The problem to be clarified is that how and why the electromagnetic wave detour its propagation path. To answer this question, we calculate the modal solution including the dispersion relation and modal function in the constituent regions denoted as (I), (II), (III), and (IV) shown in Fig. 1(c). Each of the regions is considered as a multiple dielectric layers enclosed by parallel metal plates, where the structure is infinite in extent along the y-axis. The transverse resonance approach is employed to calculate the dispersion characteristics of waveguide modes. Figure 5(a)–5(d) depict the dispersion relation of waveguide modes supported in the four regions, respectively. Notably, since the structure is symmetric with respect to the y-axis, the dispersion curves contain OCBS (open-circuit bisection, or even-) modes and SCBS (short-circuit bisection, or odd-) modes denoted in the figure. However, only the OCBS mode is excited because that the probe locates at the central position. The vertical axis of the dispersion diagram is the effective dielectric constant, which is defined as $\epsilon_{eff} = (k_y/k_o)^2$, where k_y is the propagation constant along the waveguide axis. Parameter k_o is the free-space wavenumber defined as $k_o = 2\pi/\lambda$, where λ is the wavelength in free space. The horizontal axis is the operational frequency (in GHz). Additionally, we also plotted the mode profile (or eigen-function) associated with the first OCBS mode at 3 GHz, shown in the inset of each subfigure. In Fig. 5(a), because that the effective dielectric constant is greater than 1.0 at 3 GHz, the x-component propagation constant (k_x) in the air region becomes a pure imaginary number. Consequently, the mode function in the air region exhibits exponentially decaying, shown in the inset. The modal functions are similar to each other in the inset of Fig. 5(b) and 5(c), because of insignificant difference in their effective dielectric constants. We may conclude that the dielectric cloak, in fact, is served as a mode converter for transforming the incident TE_{10} mode into the mode function with twin peaks near the waveguide sidewalls. The width and relative dielectric constant of each dielectric slab determine the type of mode to be generated. Moreover, the length of each dielectric slab dominates the mode transition and mainly affects the return loss.

We have carried out the sensitivity calculation of a single parameter for the length, width and relative dielectric constant of the dielectric slabs, respectively. For easy observing, the range of variation of the transmission coefficient (S_{21}) against the parameter under sweeping is drawn. Therefore, the curve with thick width indicates that the transmission coefficient is sensitive to the

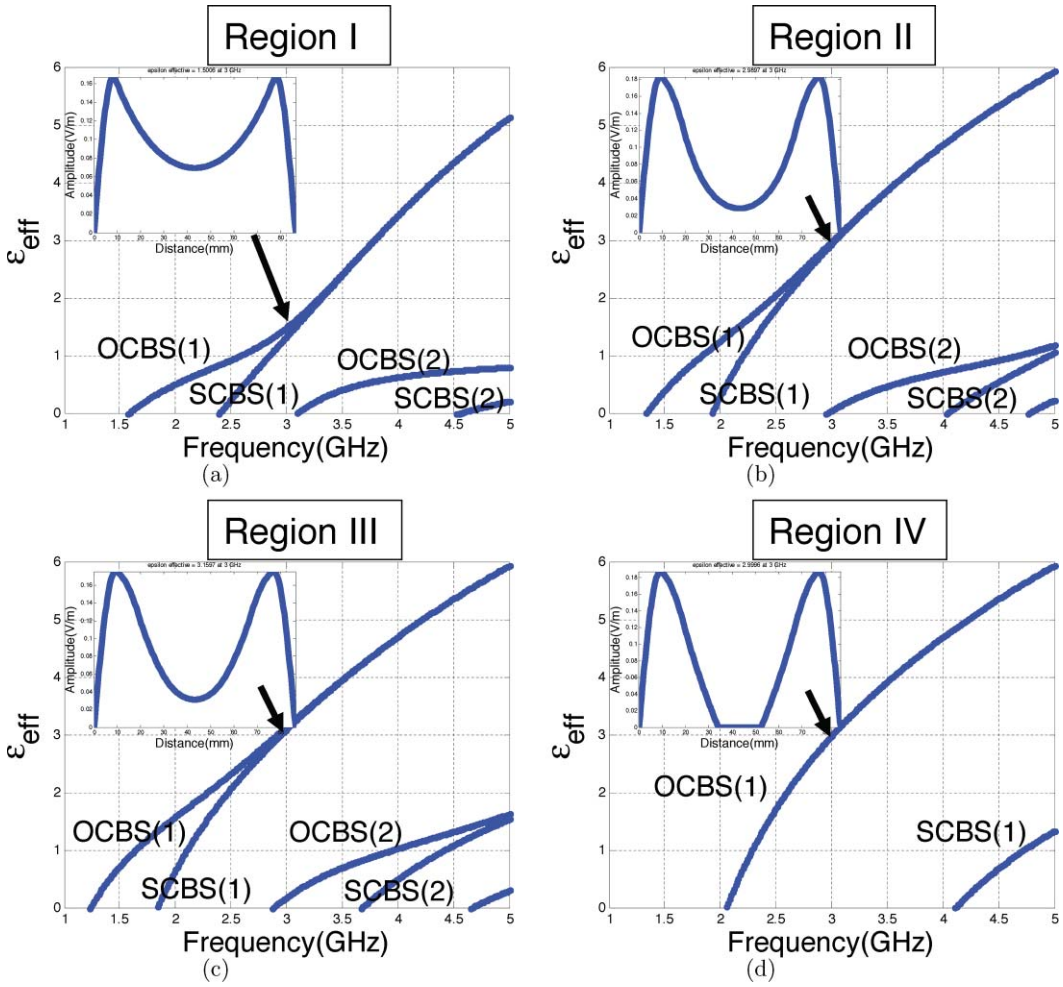

FIG. 5. Dispersion relation and fundamental modal profile of each region described in Fig. 1 and corresponding parameters such as length and width are listed in Table I. The index after the OCBS (SCBS) is defined as the order of the even (odd) modes. For example, OCBS(1) is denoted as the first even mode and SCBS(2) is the second odd mode.

change of the parameter. Figure 6(a)–6(c) show the sensitivity analysis for the parameter l_1, l_2 and l_3, respectively, while the other parameters are fixed. The detail parameters are given in the caption of each sub-figure. Additionally, the sensitivity analyses of the widths and relative dielectric constants of the three dielectric slabs are also calculated and shown in Fig. 7(a)–7(c) and Fig. 8(a)–8(c), respectively.

From these figures, we may observe that the transmission coefficient is more sensitive to the width and relative dielectric constant of the RT6010 than those of the Acrylic and FR4. Returning to the dispersion relation and modal profile shown in Fig. 5, we know that the field strength concentrates around the region with highest relative dielectric constant. Therefore, a perturbation on the width and relative dielectric constant of the RT6010 certainly changes its dispersion characteristic. Contrarily, the change in the length of RT6010 affects S_{21} insignificantly since the dispersion relation and modal profile remain the same. Generally, the first higher-order OCBS mode is excited as the frequency is greater than about 3 GHz in region I, II and III; however, it is evanescent in region IV. Since the first higher-order mode is in the vicinity of the cutoff frequency, it carries far less energy than that of the fundamental mode. Although not shown here, only the first higher-order mode is excited and the change on the position and profile is insignificant for the sensitivity analysis in Fig. 7 and 8. Therefore, the influence from the excitation of higher-order mode is not obvious in the frequency rage of operation.

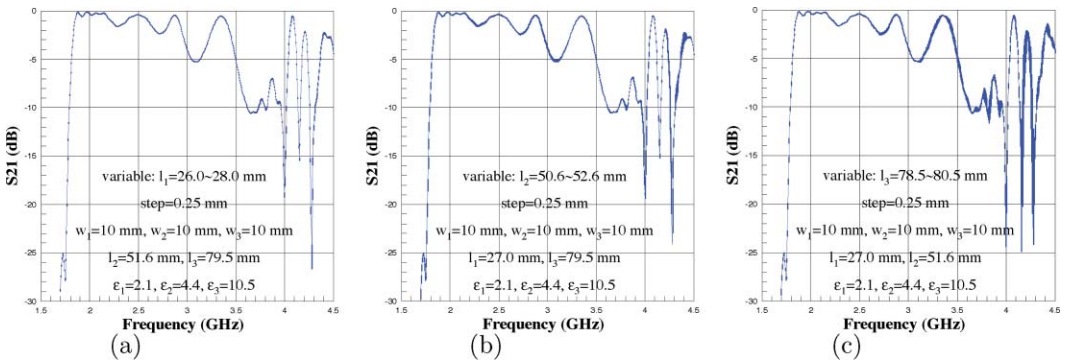

FIG. 6. Sensitivity analysis for length of each dielectric slab l_1, l_2 and l_3 respectively. The sweeping range and step of parameter are given in the figure while other parameters are fixed as indicated in Table I.

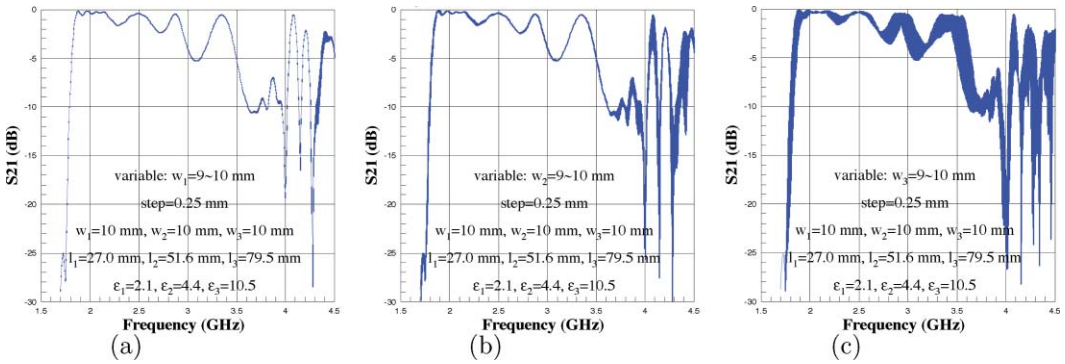

FIG. 7. Sensitivity analysis for width of each dielectric slab w_1, w_2 and w_3 respectively. The sweeping range and step of parameter are given in the figure while other parameters are fixed as indicated in Table I.

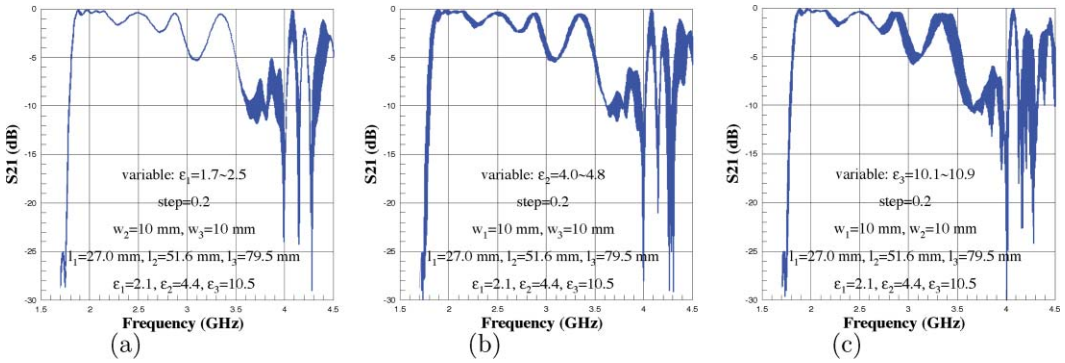

FIG. 8. Sensitivity analysis for relative dielectric constant of each dielectric slab ϵ_1, ϵ_2 and ϵ_3 respectively. The sweeping range and step of parameter are given in the figure while other parameters are fixed as indicated in Table I.

V. CONCLUSIONS

A broadband cloaking structure comprised of composite dielectrics for cloaking a metallic block in a waveguide was demonstrated numerically and experimentally. The physical consequence of cloaking is attributed to the path deformation for the electromagnetic wave propagation through the dielectric cloak. Additionally, the theory of mode conversion was developed to interpret the cloaking phenomenon.

ACKNOWLEDGMENTS

The corresponding author of this paper wishes to acknowledge CST™ for their support in providing software for numerical simulation.

[1] A. Alù and N. Engheta, Phys. Rev. E **72**, 016623 (Jul. 2005).
[2] A. Alù and N. Engheta, Opt. Express **15**, 3318 (Mar. 2007).
[3] A. Alù and N. Engheta, Phys. Rev. Lett. **100**, 113901 (Aug. 2008).
[4] G. Milton and N.-A. Nicorovici, Proceedings of the Royal Society A: Mathematical, Physical and Engineering Science **462**, 3027 (Oct. 2006).
[5] N. A. Nicorovici, G. W. Milton, R. C. Mcphedran, and L. C. Botten, Opt. Express **15**, 6314 (May 2007).
[6] U. Leonhardt, Science **312**, 1777 (Jun. 2006).
[7] U. Leonhardt, New Journal of Physics **8**, 118 (Jul. 2006), ISSN 1367-2630.
[8] J. B. Pendry, Phys. Rev. Lett. **85**, 3966 (Oct. 2000).
[9] J. Pendry, D. Schurig, and D. Smith, Science **312**, 1780 (Jun. 2006), ISSN 1095-9203.
[10] D. Schurig, J. J. Mock, B. J. Justice, S. A. Cummer, J. B. Pendry, A. F. Starr, and D. R. Smith, Science **314**, 977 (Nov. 2006).
[11] P. Alitalo, O. Luukkonen, L. Jylha, J. Venermo, and S. Tretyakov, IEEE Transactions on Antennas and Propagation **56**, 416 (Feb. 2008), ISSN 0018-926X.
[12] P. Alitalo, F. Bongard, J. Zürcher, J. Mosig, and S. Tretyakov, Appl. Phys. Lett. **94**, 014103 (Jan. 2009).
[13] W. Cai, U. K. Chettiar, A. V. Kildishev, and V. M. Shalaev, Nat. Phonton. **1**, 224 (Apr. 2007).
[14] R. C. Rumpf, M. A. Fiddy, and M. E. Testorf, Opt. Express **15**, 4735 (Apr. 2007).
[15] M. Silveirinha, A. Alù, and N. Engheta, Phys. Rev. E **75**, 036603 (Mar. 2007).